NRC Research Press

ARTICLE

Molecular modeling and inhibitor docking analysis of the Na^+/H^+ exchanger isoform one[1]

Debajyoti Dutta and Larry Fliegel

Abstract: Na^+/H^+ exchanger isoform one (NHE1) is a mammalian plasma membrane protein that removes intracellular protons, thereby elevating intracellular pH (pH_i). NHE1 uses the energy of allowing an extracellular sodium down its gradient into cells to remove one intracellular proton. The ubiquitous protein has several important physiological and pathological influences on mammalian cells as a result of its activity. The three-dimensional structure of human NHE1 (*h*NHE1) is not known. Here, we modeled NHE1 based on the structure of *Mj*NhaP1 of *Methanocaldoccocus jannaschii* in combination with biochemical surface accessibility data. *h*NHE1 contained 12 transmembrane segments including a characteristic Na^+/H^+ antiporter fold of two transmembrane segments with a helix – extended region – helix conformation crossing each other within the membrane. Amino acids 363–410 mapped principally to the extracellular surface as an extracellular loop (EL5). A large preponderance of amino acids shown to be surface accessible by biochemical experiments mapped near to, or on, the extracellular surface. Docking of Na^+/H^+ exchanger inhibitors to the extracellular surface suggested that inhibitor binding on an extracellular site is made up from several amino acids of different regions of the protein. The results present a novel testable, three-dimensional model illustrating NHE1 structure and accounting for experimental biochemical data.

Key words: molecular modeling, *Mj*NhaP1, Na^+/H^+ exchanger, NhaA, NHE1.

Résumé : L'échangeur Na^+/H^+ NHE1 est une protéine de la membrane plasmique des mammifères qui enlève les protons intracellulaires, élevant ainsi le pH intracellulaire (pH_i). NHE1 utilise l'énergie générée par l'entrée spontanée dans les cellules d'un sodium extracellulaire par gradient pour faire sortir un proton intracellulaire. Cette protéine ubiquiste exerce une influence importante sur les plans physiologiques et pathologiques dans les cellules de mammifères conséquemment à son activité. La structure tridimensionnelle de NHE1 humain (*h*NHE1) n'est pas connue. Les auteurs ont modélisé ici NHE1 à partir de la structure de *Mj*NhaP1 de *Methanocaldococcus jannaschii* en combinaison avec les données biochimiques d'accessibilité de la surface. Le transporteur *h*NHE1 comprenait 12 segments transmembranaires dont un repli caractéristique de l'antiport Na^+/H^+, formé de deux segments transmembranaires dans une conformation hélice – région étendue – hélice qui se croisent à l'intérieur de la membrane. Les acides aminés 363–410 ont été cartographiés principalement à la surface extracellulaire en tant que boucle extracellulaire (EL5). Une forte prépondérance d'acides aminés accessibles à la surface selon des expériences biochimiques était cartographiée à proximité ou sur la surface extracellulaire. L'amarrage d'inhibiteurs de l'échangeur Na^+/H^+ à la surface extracellulaire suggérait que la liaison de l'inhibiteur sur un site extracellulaire implique plusieurs acides aminés de différentes régions de la protéine. Les résultats présentent un nouveau modèle tridimensionnel vérifiable qui illustre la structure de NHE1 et explique les données biochimiques expérimentales. [Traduit par la Rédaction]

Mots-clés : modélisation moléculaire, *Mj*NhaP1, échangeur Na^+/H^+, NhaA, NHE1.

Introduction

Membranes are key to cellular function. They separate cells from the extracellular environment and allow cells to maintain intracellular compartments of specific content. The plasma membrane of eukaryotic cells provides a barrier to ions permitting, for example, a relatively low intracellular sodium level and a high intracellular potassium relative to the extracellular milieu of mammalian cells. However, at the same time, the plasma membrane restricts the removal of cations such as protons, which accumulate as a result of cellular metabolism. One protein that removes intracellular protons, and thereby elevates intracellular pH (pH_i), is the mammalian Na^+/H^+ exchanger isoform one (NHE1). NHE1 is an 815 amino acid plasma membrane protein ubiquitous in mammalian cells. It consists of a membrane domain of about 500 amino acids and an internal cytosolic regulatory domain (Fig. 1A). NHE1 allows an extracellular sodium down its gradient into the cell and removes one intracellular proton. It thus maintains and elevates pH_i while protecting cells from metabolism-induced acidification. NHE1 also responds actively to osmotic stress, thereby aiding in regulation of cell volume (Fliegel 2005; Hendus-Altenburger et al. 2014). There are 10 isoforms of Na^+/H^+ exchangers that are different gene products. Isoform one, the ubiquitous NHE1, has several important physiological and pathological influences on mammalian cells as a result of its activity (Fliegel et al. 1991, 1993; Orlowski et al. 1992; Takaichi et al. 1992; Fliegel 1999; Orlowski and Grinstein 2004; Lee et al. 2008; B.L. Lee

Received 18 May 2018. Accepted 13 July 2018.

D. Dutta and L. Fliegel. Department of Biochemistry, University of Alberta, Edmonton, AB T6G 2H7, Canada.
Corresponding author: L. Fliegel (email: lfliegel@ualberta.ca).

[1]This Article is one of a selection of papers from the 2018 CSMB Conference.

Corrections were made to the e-First version of this paper on 6 May 2019 prior to the final issue publication. The current online and print versions are identical and both contain the corrections.

Fig. 1. (A) Simplified schematic model of NHE1 illustrating the general transport domain and intracellular regulatory domain. (B) Sequence alignment of *h*NHE1 and *Mj*NhaP1. NHE1_SS denotes the secondary structure prediction where red denotes an alpha helix and yellow denotes a beta sheet. NHE1_TM indicates the position of predicted transmembrane helices (gray). Secondary structure helical elements on the *Mj*NhaP1 structure are denoted using red. Final transmembrane segments in the predicted *h*NHE1 structure are denoted using bold numbers. "GLRG" indicates the position of this motif. "DP" indicates the position of the A(V/T)DPV) motif. "R" indicates the positively charged residue of TM10 (equivalent to the Lys300 of *Ec*NhaA). "ND" indicates the ND motifs of TM-7. [Color online.]

et al. 2013). In myocardial disease, elevated NHE1 activity acts as a trigger in both heart hypertrophy and ischemia reperfusion damage (Karmazyn et al. 1999; Karmazyn 2013). NHE1 is also important in breast cancer, where elevated activity can trigger metastasis (Reshkin et al. 2014; Amith and Fliegel 2016, 2017). In animal models, NHE1 inhibitors have demonstrated cardioprotective properties during ischemia reperfusion treatment episodes in the myocardium (Karmazyn 2013). In addition, NHE1 inhibition has been shown to suppress metastasis of breast cancer cells (Amith et al. 2016). There has therefore been a great deal of interest in the development of clinically useful NHE inhibitors, and although the concept of NHE inhibitors as a therapeutic agent remains sound, off target actions of one type of inhibitor prevented successful outcomes in a clinical trial (Karmazyn 2013). The *h*NHE1 protein is 815 amino acids long. The N-terminal 500 amino acids form the membrane transport domain, while the C-terminal balance forms a regulatory domain that modulates activity of the membrane domain (B.L. Lee et al. 2013).

Given that NHE1 plays an important role in human pathology and physiology, there has been a great deal of interest in determining the structure of the protein, both to determine its mechanism of transport and to facilitate the development of clinically useful inhibitors. This manuscript describes developments in characterization of the structure of the NHE1 protein from initial topology models to more recent modeling. We also present a new model of the human NHE1 (*h*NHE1) protein based on a combination of biochemical experiments and molecular modeling and based on the recently deduced crystal structure of the Methanococcus Na^+/H^+ exchanger. The three-dimensional model takes into account recent biochemical accessibility experiments.

The Na^+/H^+ exchanger family: recent advances in structure determination

Transmembrane (TM) exchange of protons for sodium ions is ubiquitous across all phyla and kingdoms and thus, NHEs play an important role in a multitude of species. The evolutionary aspects of NHEs were last reviewed by Brett et al. (2005). They divided up the monovalent cation proton antiporter (CPA) superfamily into CPA1, CPA2, and NaT-DC (sodium-transporting carboxylic acid decarboxylase) families, which each had unique bacterial ancestors. The CPA1 family transports Na^+, Li^+, K^+, or Rb^+ in electroneutral exchange for a proton and includes mammalian NHE1-9. The CPA2 family can catalyze electrogenic activity, includes Na^+, K^+/H^+ exchangers, and includes the well-known antiporter *Escherichia coli* NhaA. It also includes the fungal antiporters and the mammalian NHA1 and NHA2 proteins that are electroneutral. The NaT-DC transporters mediate the TM export of — one or two Na^+s in exchange for an extracellular H^+ as part of a multiprotein complex catalyzing the decarboxylation of oxaloacetate, malonyl-CoA, or glutaconyl-CoA.

Not surprisingly, the greatest progress has been made on elucidation of Na^+/H^+ exchanger structures of the bacterial transporters that have proven easier to overproduce and crystallize. We (Dutta and Fliegel 2018) and others (Hendus-Altenburger et al. 2014) reviewed progress on the structure of bacterial plasma membrane antiporters, which is summarized here. The structures of four plasma membrane Na^+/H^+ antiporters, NhaA of *E. coli*, (Hunte et al. 2005), NapA of *Thermus thermophilus* (C. Lee et al. 2013), *Mj*NhaP1 of *Methanocaldoccocus jannaschii* (Paulino and Kühlbrandt 2014), and *Pa*NhaP of *Pyrococcus abyssi* (Wöhlert et al. 2014) are known. The initial structure solved, that of *E. coli* NhaA, led to the idea that Na^+/H^+ antiporters have a novel fold that consists of two TM segments with a helix – extended region – helix conformation, TM4 and TM11. These cross to make the NhaA fold. *Ec*NhaA was also found to be a dimer of two 12 TM helices per protomer with both N- and C-terminal cytoplasmic tails. It had a dimerization or scaffolding subdomain and a six-helix bundle cylindrical transport subdomain (Hunte et al. 2005; Padan 2014). The "*Ec*NhaA fold" (Padan 2014) contributes to the cation binding site and allows for rapid conformational changes that occur in transport. This catalytic region is in the middle of the membrane. The antiparallel unfolded regions lie midmembrane between the helical regions. Where these unfolded regions cross each other, the helices surrounding the unfolded regions have a charge imparted from the helix dipoles midmembrane. This charge is neutralized by a charged polar amino acid within the membrane. The unfolded region of TM4 undergoes conformational changes with varying physiological pH and several of the conserved and functionally important residues of TM4 have been suggested to line the cationic passage channel, according to results of mutagenesis experiments (Rimon et al. 2012). *Ec*NhaA is active at alkaline pH (>7.5) to extrude one Na^+ in exchange for two H^+s. Clusters of titratable groups near the cytoplasmic funnel entrance of the antiporter may be part of the pH sensor (Olkhova et al. 2006) altering activity in response to pH. Another suggestion for the mechanisms of NhaA activation is that it involves a net charge switch of a pH sensor at the entrance of the cytoplasmic funnel and opening of a hydrophobic gate at the end of the funnel (Huang et al. 2016).

The NhaA fold is present in *Tth*NapA (C. Lee et al. 2013), *Mj*NhaP1 (Goswami et al. 2011), and *Pa*NhaP (Wöhlert et al. 2014). They have an additional TM helix N-terminal to the fold but have discontinuous helices 5 and 12, which correspond to 4 and 11 of *Ec*NhaA (Wöhlert et al. 2014). *Ec*NhaA is a dimer. There are dimer contacts with extracellular beta strands and TM1, TM9, TM6, and TM7. Helices 6 and 7 form an alpha hairpin at the dimer interface (Padan et al. 2015). In *Ec*NhaA, a beta sheet on the periplasmic side of the membrane is also important in dimerization (Rimon et al. 2007). *Mj*NhaP1 is a dimer like NhaA but the dimer contacts are different. The two peptides are held together by tight helix–helix interactions across an extensive, probably hydrophobic, contact surface at the dimer interface (Goswami et al. 2011).

Topology of *h*NHE1

The topology of the *h*NHE1 isoform of the Na^+/H^+ exchanger has been the subject of some debate. The first comprehensive model based on biochemical analysis was that of Wakabayashi et al. (2000). They did a thorough analysis using cysteine-scanning accessibility and suggested a 12-TM segment model. Of note, TM1 was amino acids 15–36 with an N-terminal that was cytosolic. It was followed by a large extracellular loop (EL) of about 70 amino acids. Additionally, amino acids 363–410 were thought to form a membrane-associated segment, EL55, which was preceded by TM9 (amino acids 341–362) and followed by TM10 (amino acids 411–432). TM 4 and TM11 were amino acids 154–176 and 449–471, respectively.

Later, an alternative three-dimensional model was proposed that was based on homology modeling with *Ec*NhaA (Landau et al. 2007). This model was similar to that of Wakabayashi and had 12 TM regions but it was suggested that amino acids 1–125 were removed by cleavage. TM9 of Wakabayashi et al. (2000) was reassigned as two short helices denoted TM7 and TM8 and reentrant

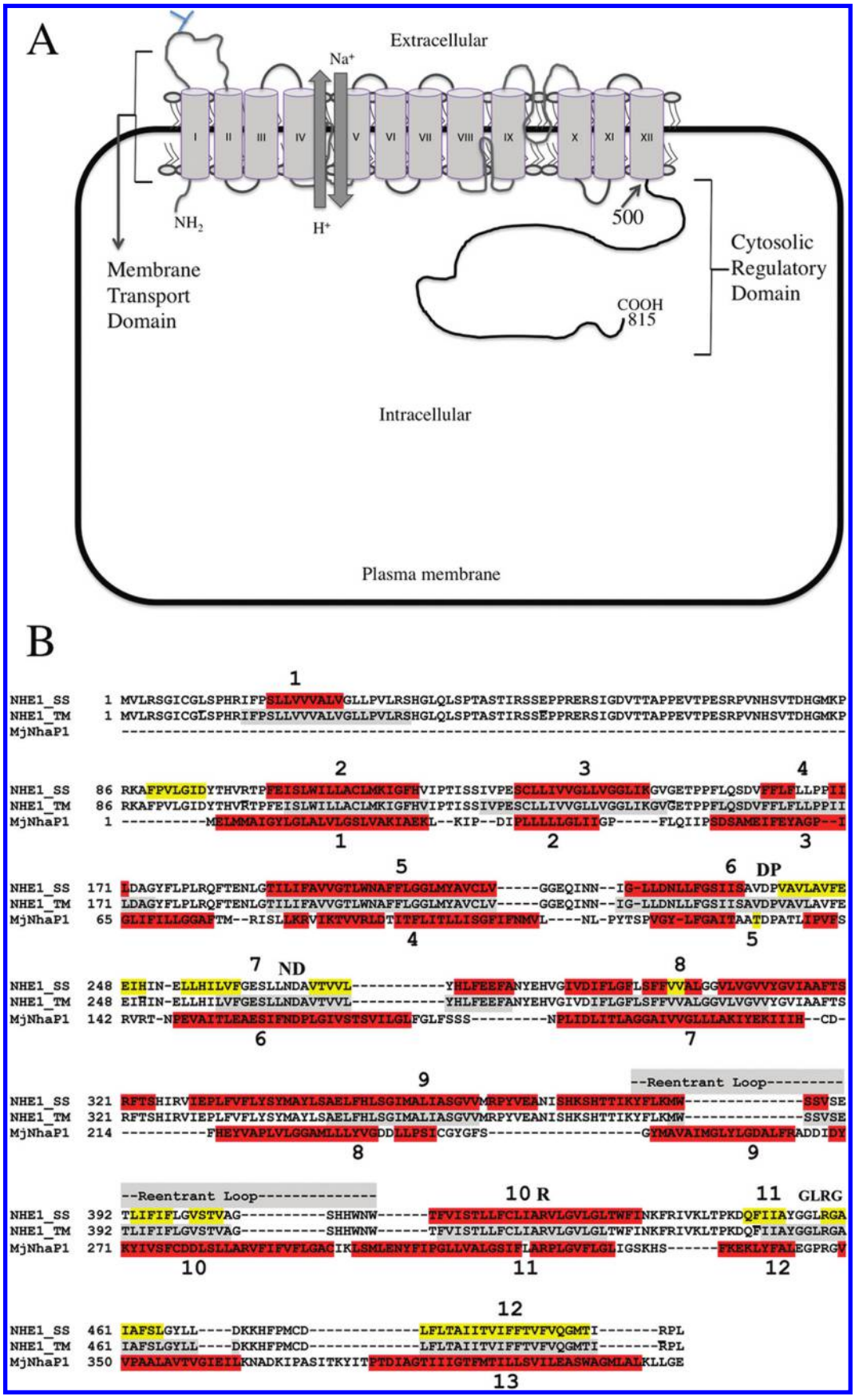

Fig. 2. Molecular model of *h*NHE1. Amino acids 12–512 are illustrated (minus EL1, amino acids 34–97). (A) Lateral view of the model. Pro12 is shown in cyan. TM4 (amino acids 155–182) is shown in yellow,TM6 (amino acids 227–248) is shown in gray, TM11 (amino acids 447–468) is shown in magenta, and EL5 (amino acids 363–410) is shown in orange. (B) As in Fig. 2A but with amino acids 480–499 and 416–434 removed for clarity. (C and D) *h*NHE1 model structure viewed perpendicular (Fig. 2C) to the membrane from the cytoplasmic side and lateral (Fig. 2D) to the membrane. N- and C-terminals are shown. TM1 (magenta)and EL5 (black), TM2 (lime green) – TM3 (pale green) – TM4 (smudge), TM8 (green), and TM9 (limon) together with EL5 form the dimerization scaffolding domain. TM5 (red) – TM6 (fire brick) – TM7 (raspberry), TM10 (deep salmon) – TM11 (warm pink), and TM12 (chocolate) form the metal transporting helix bundle. The helices across the discontinuous helix regions of TM6 and TM11 are named TM6a (N-terminal)/TM6b (C-terminal) and TM11a (N-terminal)/TM11b (C-terminal), respectively. TM segments are labeled. (E) Lateral view of TM4 (green), TM6 (magenta), and TM11 (yellow). (F) Surface accessible residues. Lateral and transparent view of *h*NHE1. *h*NHE1 TM4 (amino acids 155–182) is shown in magenta, TM11 (amino acids 447–468) is shown in yellow, and EL5 (amino acids 363–410) is shown in grey. Amino acids that have been demonstrated to be accessible on the cell surface when altered to Cys (and with the protein still active) are colored red and side chains are shown. Selected amino acids are labeled. Surface accessible amino acids from previous reports (Wakabayashi et al. 2000; Slepkov et al. 2005; Reddy et al. 2008; Liu et al. 2015; Tzeng et al. 2010) are E151, T152, P153, F161, T183, E184, E217, Q218, I219, N220, N221, N227, I233, F277, E279, F280, A281, Y283, E284, H285, S324, H325, S351, Y366, V367, E368, A369, I371, H373, K374, S375, H376, T377, S401, T402, H407, H408, and W409. [Color online.]

segment EL5 was reassigned as TM9 (amino acids 374–398). The last three TM segments were the same in both models.

Our own (Liu et al. 2015) followup work to these two studies suggested that the essential features of the Wakabayashi model were correct. We examined the cell surface accessibility of amino acids in the proposed first EL (EL1) (amino acids 36–106). A fully active cysteine-free NHE1 protein was made and we used cysteine scanning mutagenesis and MTSET labeling combined with cell surface biotinylation of this protein to determine accessibility of residues mutated to cysteine. Results showed that amino acids within this region occurred in the mature protein that was present on the extracellular surface. Additionally, by using a combination of site-specific mutagenesis and cell surface labeling, we showed that NHE1 protein with the Asn75 glycosylation site was present on the cell surface. Using the same techniques, we also examined surface accessibility of the downstream amino acids of the contentious sequence amino acids 363–410. We (Liu et al. 2015) found that amino acids 366, 369, 377, 401, and 402 are accessible from the extracellular surface, which agreed with the earlier results that used similar techniques and showed that 10 other amino acids in this segment are accessible extracellularly (Wakabayashi et al. 2000). Thus, a total of 15 amino acids within this segment are accessible to extracellular labeling when changed to Cys. Another study (Jinadasa et al. 2015) also examined amino acids of this region and their results were more supportive of the Wakabayashi model. Thus, empirically obtained biochemical data from three different laboratories support the idea that amino acids 363–410 are EL5 with amino acids 341–362 preceding it as TM9. Nevertheless, this left only a two-dimensional model of the *h*NHE1 protein.

Another study (Nygaard et al. 2011) attempted to make a three-dimensional model of *h*NHE1 threaded on the structure of NhaA. They attempted to assign comparable roles for Asp172 and Arg425 with the important functional residues of Nha, Asp133, and Lys300. Recently, however, another report (Călinescu et al. 2017) showed that mutation of Lys300 of *Ec*NhaA to several amino acids did not prevent electrogenic transport. And while it was suggested that mutation of these human residues should cause severe disruption of catalytic activity, mutation of Asp172 to Cys decreased activity mostly due to effects on reduced protein expression and targeting (Slepkov et al. 2005), and mutation of Asp172 to Asn only had a minor effect on NHE1 activity (Slepkov et al. 2007). This does not agree with the proposed role of Asp172 in screening a helix dipole. Their model did, however, predict that amino acids 363–410 are on the extracellular surface of the protein.

The development of new and improved inhibitors against *h*NHE1 can be facilitated by knowledge of the details of the atomic structure of the protein. However, obtaining the atomic structure of the entire mammalian NHE1 protein remains a challenge as yet unmet. On the other hand, computationally predicted models can still provide useful information when the atomic structure is not available (França 2015). While this approach has validity, we suggest that structural modeling should take into account empirically determined biochemical data, when available, rather than being based solely on computer modeling that is untested. *Ec*NhaA is only 15% identical and 31% similar to *h*NHE1, and among other new Na^+/H^+ exchanger structures elucidated, the sequence of *Mj*NhaP1 (Goswami et al. 2011) is more similar to *h*NHE1 with 20% identity and 38% similarity. Additionally, both *h*NHE1 and *Mj*NhaP1 show similar pH profiles for activity being activated by decreases in pH_i (Hellmer et al. 2002), while that of *E. coli* is quite different from *h*NHE1 (Dutta and Fliegel 2018). Recently, we predicted the structure of the plasma membrane Na^+/H^+ antiporter for plant and yeast proteins using a procedure that is based on an inclusive sequence alignment (Ullah et al. 2016; Dutta et al. 2017; Dutta and Fliegel 2018). Here, we take a similar approach to build a *h*NHE1 structure based on *Mj*NhaP1.

Methods

Building a *h*NHE1 model

Alignment

*h*NHE1 sequence shows 20% sequence identity with *Mj*NhaP1 in the membrane domain, higher than that of *Ec*NhaA, which is 15% identical. Therefore, *Mj*NhaP1 (PDB 4CZB) was used as a template to build the *h*NHE1 model. Multiple and pairwise sequence alignment was done as described earlier (Dutta and Fliegel 2018) and is shown in Fig. 1B. Briefly, the MAFFT server (Katoh and Standley 2013) was used for multiple and pairwise sequence alignment. Secondary structure prediction was done using the PSIPRED server (Buchan et al. 2013). TM segment assignment was performed using TMHMM (Möller et al. 2001) and the TMpred server (Hofmann and Stoffel 1993). In the alignment, we included only amino acids 96–520 of *h*NHE1 for a pairwise sequence alignment with amino acids 1–415 *Mj*NhaP1. These residues contain the entire membrane domain of *h*NHE1 except for the first TM segment (TM1) and EL1. TM segment predictions of *h*NHE1 were compared with the known secondary structure elements of *Mj*NhaP1 structure (Paulino and Kühlbrandt 2014). The alignment of TM9 and the EL5 region was manually edited based on their predicted secondary structure, NMR structural data (Reddy et al. 2008), and amino acid accessibility data (Wakabayashi et al. 2000; Liu et al. 2015).

Three-dimensional modeling

To obtain a three-dimensional structure of the *h*NHE1 protein, a model was built using MODELLER 9.v2 (Šali and Blundell 1993). The NhaA fold has been shown to be present in several types of Na^+/H^+ exchanger including NhaA of *E. coli* (Hunte et al. 2005), NapA of *T. thermophilus* (C. Lee et al. 2013), *Mj*NhaP1 of *M. jannaschii* (Paulino and Kühlbrandt 2014). and PaNhaP of *P. abyssi* (Wöhlert et al. 2014). Therefore, the first round of modeling was performed with default parameters of MODELLER 9.v2 with an assumption

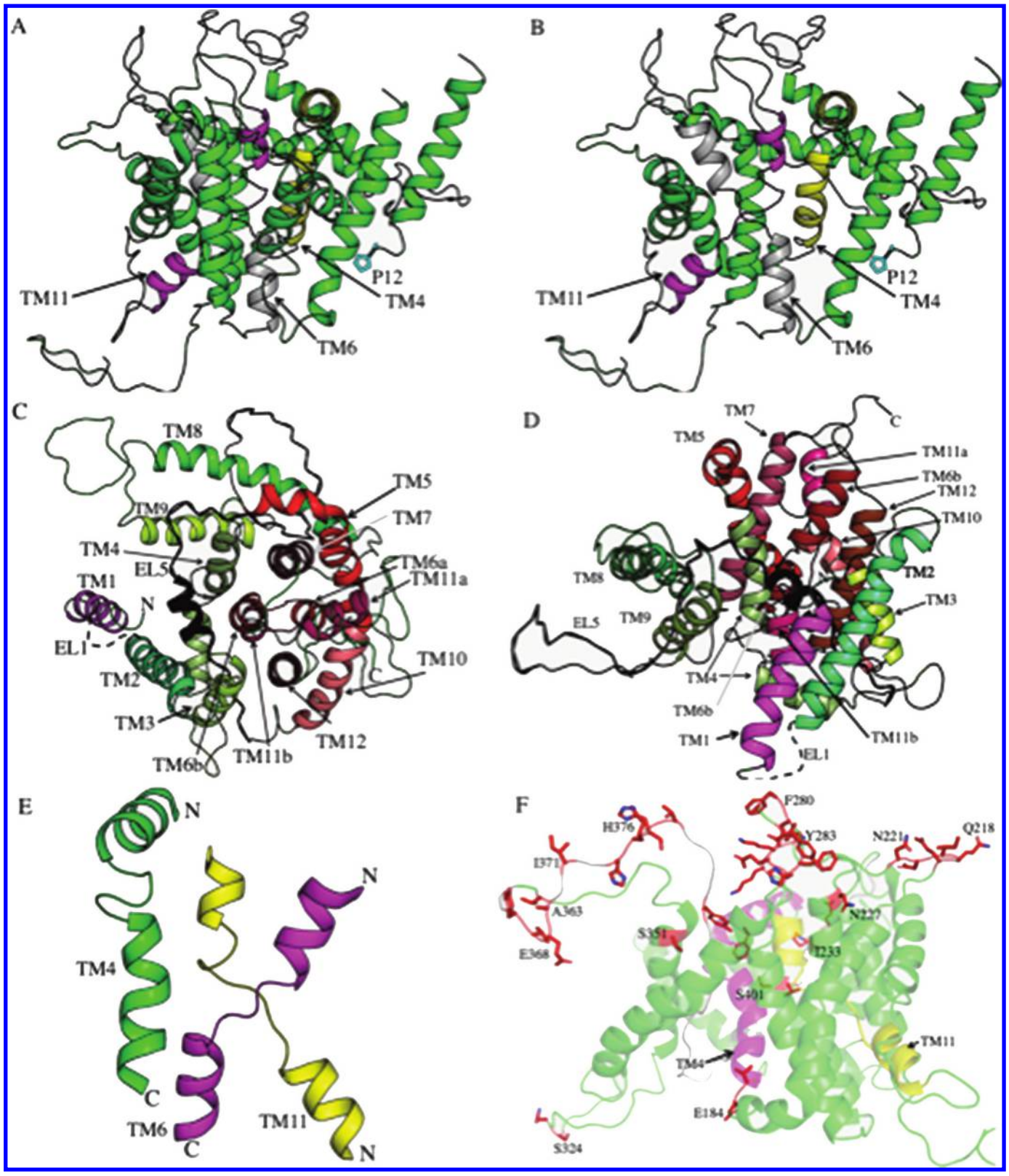

that relative positions of the TM helices of *h*NHE1 would be similar to those of *Mj*NhaP1. The initial 50 structures of *h*NHE1 contained TM2–TM12 (residues 96–250). From these structures, one that closely matched the predicted TM spans was chosen for further structural editing using COOT (Emsley et al. 2010). The C-terminal region of TM9 (349–365) was built from the NMR structure (PDB 2K3C) (Reddy et al. 2008). Other structural editing of the reentrant loop containing residues 366–415 was built ab initio (Emsley et al. 2010) based on cysteine scanning mutagenesis studies for surface accessibility data (Wakabayashi et al. 2000; Slepkov et al. 2005; Reddy et al. 2008; Tzeng et al. 2010; Jinadasa et al. 2015; Liu et al. 2015).

Because there is no known structural template for EL1 (amino acids 35–95) and TM1, we incorporated TM1 (amino acids 12–34) separately into the model. The structure of TM1 (12–34) was obtained from a previously published *h*NHE1 model (Nygaard et al. 2011) and submitted to the HADDOCK server (van Zundert et al. 2016), which contains protein–protein docking software. As the NHE1 protein is known to be a dimer (Fafournoux et al. 1994; Hisamitsu et al. 2006; Moncoq et al. 2008), the relative position of TM1 on the dimer interface of the NHE1 model was also predicted using HADDOCK (van Zundert et al. 2016) with the assumption made that TM1 should be present at the dimerization interface. TM1 has earlier been shown to be present at the dimerization interface in all Na^+/H^+ antiporter structures reported (Hunte et al. 2005; C. Lee et al. 2013; Paulino and Kühlbrandt 2014; Wöhlert et al. 2014). The second assumption was that TM1 should be in proximity to TM2, which is also typical of the previously reported NHE structures. With these two assumptions, hydrophobic residues from TM1 (Leu20, Ala24, Val31) and TM2 (Leu107, Leu114) were defined as "active residues" that can take part in TM1–TM2 interactions. Several potential interacting clusters were obtained from the HADDOCK analysis. However, the docking output of TM1 on the dimer interface was chosen based on two criteria. One was the orientation of the helix; the N-terminal of the first helix should be located on the same cytosolic side as the C-terminal of the protein. The second criterion was the selection of the populated cluster of TM1 at the dimer interface involving the most hydrophobic interactions, with buried surface area. Two potential clusters emerge from the docking results. These clusters (A and B) are shown in Fig. 1S[2]. Between two potential positions, cluster A has the highest HADDOCK score (–80.8 ± 8.5) followed by cluster B (–76 ± 4.2). The entire TM1-docked NHE1 structure was checked manually for any potential clashes and the Ramachandran plot improved using COOT (Emsley et al. 2010). TM1 from cluster A was used further due to several reasons. First, the cluster has the highest computational score. Second, TM1 in cluster A is relatively better packed with the rest of the TM domain. The structure was refined using the ModRefiner server (Xu and Zhang 2011). Finally, the quality of the model was checked using the software RAMPAGE (Lovell et al. 2003). The final model contains 89.4% favored regions, 8.4% allowed region, and 2.3% disallowed region in the Ramachandran plot.

Docking of NHE1 inhibitors

To explore the *h*NHE1 inhibitor binding site, we docked *h*NHE1 inhibitors computationally to the NHE1 model structure. The coordinates of the ligand EIPA (5-(*N*-ethyl-*N*-isopropyl)amiloride) and other ligands (5-(*N*,*N*-hexamethylene)amiloride (HMA), HOE694, and amiloride) were obtained from the PubChem database (https://pubchem.ncbi.nlm.nih.gov/) and format converted using UCSF Chimera (Pettersen et al. 2004). For docking studies, both ligand and protein were prepared using AutoDock Tools v1.5.6 (Morris et al. 2009). The ligand was added with all hydrogens to calculate Gasteiger charges and then nonpolar hydrogens were merged. Macromolecules were prepared by adding polar hydrogen and then the Kollman United Atom charges were assigned. AutoDock Tools was also used to prepare a grid box for blind docking that included the entire protein surface open to either side of the membrane. Any flexible bonds on the ligand were selected using AutoDock Tools. Docking of the inhibitor was performed using Autodock Vina 1.1.2 (Trott and Olson 2010). A default exhaustiveness level was chosen to perform the docking run. To improve the docking results, the grid box was narrowed down stepwise. Initially, a blind dock was performed with a box size 30 × 30 × 30. Then the initial docking regions were included in the second docking with a smaller grid box with dimension 22 × 22 × 22. Similar protocols were used to dock other *h*NHE1 inhibitors: amiloride, cariporide, HOE694, and HMA. RMSD was determined using Cα superposition in Pymol.

Results and discussion

NHE1 and *Mj*NhaP1 alignment

Here, we aligned amino acids 96–520 of *h*NHE1 with amino acids 1–415 of *Mj*NhaP1 as described above. The *h*NHE1 sequence shows more (20%) sequence identity with *Mj*NhaP1 in the membrane domain in comparison with *Ec*NhaA (15% sequence identity). Residues 96–520 of *h*NHE1 do not contain TM1 and EL1. In the multiple sequence alignment (Fig. 1B), the first TM segment of *Mj*NhaP1 is aligned with the second TM segment of *h*NHE1. The orientations of these helices are in agreement. The first TM segment of *Mj*NhaP1 is oriented from the outside to inside (Paulino and Kühlbrandt 2014), which is the same orientation as the second TM segment of the *h*NHE1. A notable disparity between the sequences is observed in reentrant loop EL5 (349–415) of *h*NHE1.

Several motifs of Na^+/H^+ exchangers have been shown to be critical in activity (Dutta and Fliegel 2018). In TMXI of Na^+/H^+ exchangers, there is a GLRG motif in the extended nonhelical region of the protein. An ND motif is found in the CPA1 antiporter family and its mutation compromises activity. A motif, TDPV, contains a critical hydroxyl on the Thr (which is sometimes a Ser) and a critical Pro. In the pair alignment, it is evident that most of these motifs critical in activity of the Na^+/H^+ antiporters are conserved. For example, the TDPV motifs of TM6 (TM5 of *Mj*NhaP1), the ND motifs of TM7 (TM8 of *Mj*NhaP1), and the GLRG motifs of TM11 (TM12 of *Mj*NhaP1) (Dutta and Fliegel 2018) are aligned and mostly conserved. In fact, overall, the only poor alignment was found across TM9, which is followed by the membrane reentrant loop EL5 (Wakabayashi et al. 2000; Liu et al. 2015).

Model description

For three-dimensional modeling of the *h*NHE1 protein, a model was built using MODELLER 9.v2 (Šali and Blundell 1993). MODELLER has been earlier used to model membrane proteins based on related templates. For example, a similar approach was used earlier with this software to generate models of fungal H^+-ATPases based on a distantly related Ca^{2+}-ATPase that shares a conserve structural fold. The resulting model closely matched the cryoEM structure of the protein (Kühlbrandt et al. 2002). Our final three-dimensional model (Fig. 2) of the NHE1 membrane domain contains 12 TM helices with both cytoplasmic N- and C-termini. The 12 TM spans are Arg14–Arg33 (TM1), Val99–Val121 (TM2), Glu131–Leu141 (TM3), Phe155–Phe182 (TM4), Leu186–Cys212 (TM5), Asn227–Glu248 (TM6), Glu253–Val272 (TM7), Gly287–Gly313 (TM8), Leu336–Met354 (TM9), Ser416–Thr433 (TM10), Lys447–Leu468 (TM11), and finally Phe480–Met497 (TM12). Figures 2A, 2B, and 2D illustrate lateral views of the model and Fig. 2C a view from the cytoplasmic side.

TM1 and EL1

The process above so far describes *h*NHE1 modeling of TM2–TM12. The N-terminal of TM1 of *h*NHE1 is cytoplasmic. TM1, although predicated to be a signal sequence, remains attached to the mature protein (Fafournoux et al. 1994; Liu et al. 2015). As noted above, TM1 modeling was from Nygaard et al. (2011) and docked independently. Therefore, it was docked separately using the HADDOCK protein–protein docking server. Although HADDOCK was designed for aqueous phase proteins, it has been used for membrane proteins with the primary prerequisite being the definition of the binding site (Rashid and Kuyucak 2012; Kaczor et al. 2013). EL1 joins TM1 with TM2 and possess one N-linked site and

[2]Supplementary data are available with the article through the journal Web site at http://nrcresearchpress.com/doi/suppl/10.1139/bcb-2018-0158.

Fig. 3. Comparison of the model structure and peptide structure of isolated segments of *h*NHE1. (A) Green, TM4 structure from NMR of the peptide (Slepkov et al. 2005); red, molecular model of TM4. (B) Green, TM6–TM7 structure from NMR of the peptide (Alves et al. 2014); red, molecular model of TM6–TM7. (C) Green, TM9 structure from NMR (Reddy et al. 2008); red, molecular model. (D) Green, TM11 structure from NMR (Lee et al. 2009); red, molecular model. [Color online.]

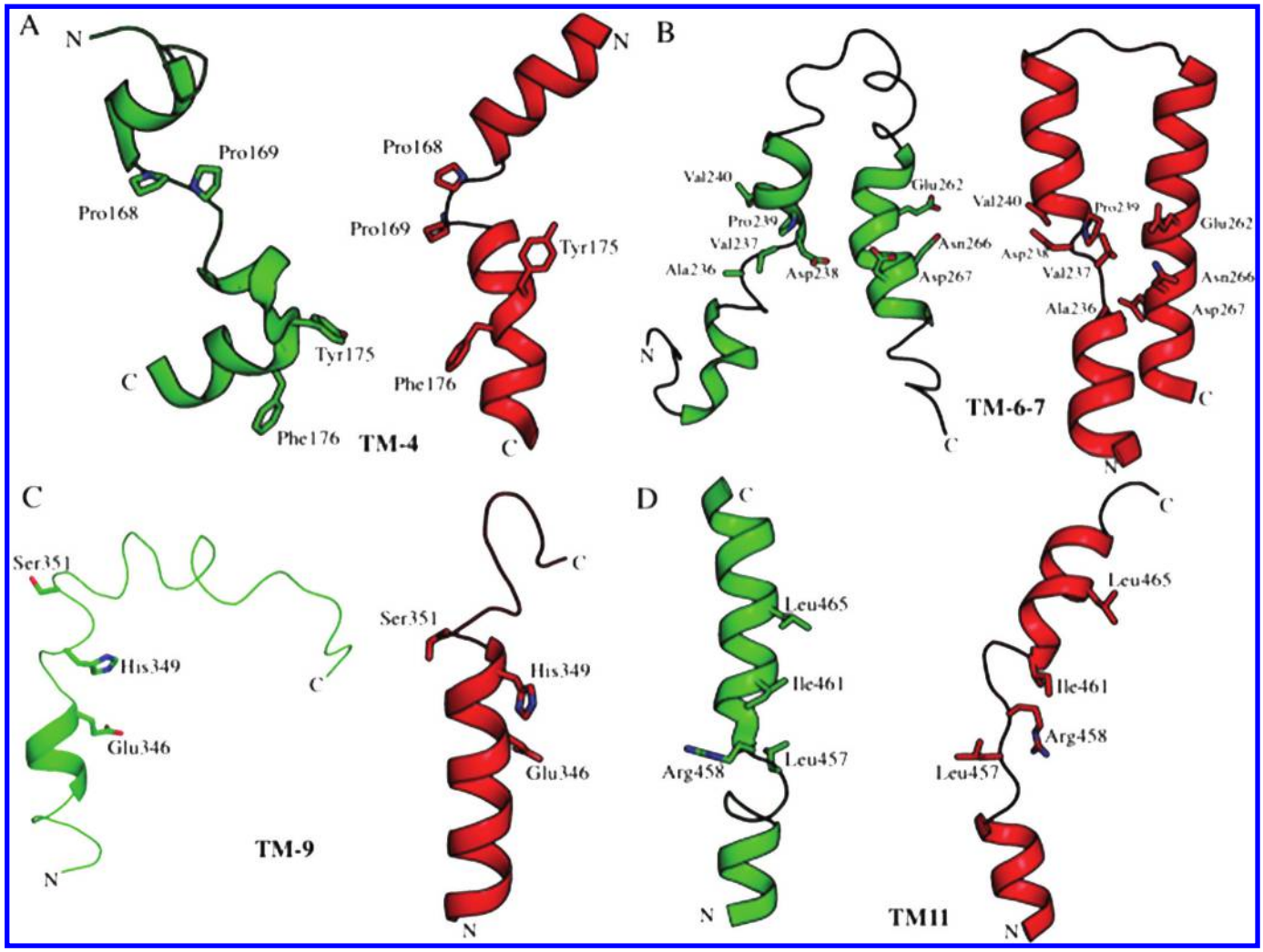

possibly O-linked glycosylation sites (Haworth et al. 1993; Counillon et al. 1994). TM1 and EL1 could not be modeled based on *Mj*NhaP1, as it does not align with the protein (Fig. 1). TM1 showed mostly hydrophobic interactions with TM2 (Fig. 2C).

TM4

Several residues of TM4 of NHE1, Phe162, Leu163, Phe167, and Gly164, are regarded as critical for inhibitor sensitivity (Counillon et al. 1993*b*, 1997; Touret et al. 2001; Pedersen et al. 2007). The NMR structure of a peptide of TM4 showed only a partly helical conformation (Slepkov et al. 2005). Our results here suggest that TM4 is a helix followed by an unwound region that is followed by a helix (Figs. 2C and 2E). The unwound region consists of the sequence 165LLPPIIL171. In comparison with *Mj*NhaP1 (Fig. 1), *h*NHE1 has an extra Pro residue (Pro168) in this segment, which can account for the extended conformation (Slepkov et al. 2007). TM4 is associated with TM6 and TM11. Spin labeling Ala173Cys of TM4 and Ile461Cys of TM11 suggested an approximate distance of 15 Å between these two residues (Nygaard et al. 2011). In our model, we found a distance of 9.5 Å between two Cα; the differences could be due to a bias created by using *Mj*NhaP1 as a template or different conformations of the protein. The template *Mj*NhaP1 structure was determined at pH 8, which may be responsible for the conformation that is reflected in our model. The predicted structure of TM4 that we found is similar to that obtained by examining the structure of a peptide of TM4 (Slepkov et al. 2005) (Fig. 3A).

TM6 and TM7

In the model, TM7 is a continuous helix whereas TM6 is a discontinuous helix and both are packed closely in the presence of other helical segments (Fig. 2C). This model structure closely resembles an NMR structure of a peptide of TM6–TM7 published earlier (Alves et al. 2014). Analysis of these two TM segments' structure (Alves et al. 2014) also showed that there was a close interaction between Val242 and Phe260, which is also found in our structure (7.7 Å C_α distance). The RMSD between the modeled TM6–TM7 and the NMR structure (PDB 2MDF) of TM6–TM7 is 4.7 A over 318 atoms. Plasma membrane Na^+/H^+ antiporters have a "TDPV" ((V/T)DPV) motif present that has a role in activity of the protein (Dutta and Fliegel 2018). In TM6, this is present in the discontinuous region in the model structure (Fig. 2E). A similar discontinuity is present in the equivalent helix of *Sp*NHE1 (Ullah et al. 2013). A peptide of TM6–TM7 was examined earlier by NMR. It has the same general structure, with TM6 having a discontinuous region (Alves et al. 2014) (Fig. 3B).

TM9

Leu336–Met354 make up TM9 in the model as a continuous helix (Fig. 2D). Assignment of these residues as a helix has been contentious in the past with one model assigning them as a helix (Wakabayashi et al. 2000) and another suggesting that they form two separate TM segments (TM7 and TM8) (Landau et al. 2007). This region is weakly conserved among Na^+/H^+ antiporters (Dutta and Fliegel 2018) and the corresponding region in *Ec*NhaA is located at the dimer interface (Padan et al. 2015). When mutated to Cys, amino acid 351 of this region is accessible to extracellular sulfhydryl labeling. Also, interestingly, a peptide of this region shows a kink around Ser351 that may indicate some mobility in this region (Reddy et al. 2008) (Fig. 3C). Mutations to TM9 can affect sensitivity towards mammalian NHE1 inhibitors (Khadilkar et al. 2001; Jinadasa et al. 2015).

TM11

In our model, TM11 is a discontinuous helix (Figs. 2C–2E). An NMR structure of a peptide of *h*NHE1, TM11 (Fig. 3D), was also a discontinuous helix (Lee et al. 2009). In other Na^+/H^+ exchanger isoforms, TM11 forms part of the NhaA fold and is believed to participate in cation transport including in NhaA and in *Sp*NHE1 (Hunte et al. 2005; Dutta et al. 2017). In the present model, the unwound region of *h*NHE1 TM11 contains the motif ^{456}GLRG^{459}. This unwound region was also found in the structure of a peptide of this region, deduced by NMR (Lee et al. 2009). The presence of an arginine (Arg458) at the center of the segment is intriguing. In mutagenesis experiments, mutation of this Arg458 to Cys caused intracellular localization of the protein and compromised activity. Mutation of Gly459 also greatly compromised activity (Lee et al. 2009). The corresponding sequence is GPRG (Fig. 1) in *Mj*NhaP1 and in *Mj*NhaP1, *Pa*NhaP, and *Tth*NapA, this Arg side chain correlates with a kink in the TM segment with a peptide backbone interaction (Goswami et al. 2011; C. Lee et al. 2013; Wöhlert et al. 2014). The structure of TM11 predicted in the model is similar to the structure of a peptide of TM11 (Fig. 2D) obtained by NMR (Lee et al. 2009).

EL5

In the model, the C-terminal (355–360) of TM9 continues as EL5 on the extracellular surface (Figs. 2C and 2D). From amino acid 361, it extends extracellularly initially including approximately amino acids 361–380. EL5 then reenters the protein core to enter the membrane twice (381–391 and 391–399). The rest of EL5 is exposed extracellularly (401–415). The modeling software suggests that residues 394–402 are helical and residues 372–389 are an extended sheet, although other secondary structure predication software (not shown) suggested that amino acids 394–402 may also be an extended sheet.

TM segment organization

Na^+/H^+ antiporters have been shown to consist of two distinct domains: a dimerization or scaffolding domain and a helix bundle or transportation domain (Hendus-Altenburger et al. 2014; Padan et al. 2015). The NHE1 model possesses an inverted topology of TM helices as reported (Hendus-Altenburger et al. 2014; Padan et al. 2015) for other Na^+/H^+ exchangers. It is arranged such that TM2–TM3–TM4 and TM8–TM9 are intertwined to make the dimerization domain whereas TM5–TM6–TM7 and TM10–TM11–TM12 form the metal transportation domain (Figs. 2C and 2D). TM5–TM6–TM7 and TM10–TM11–TM12 are inverted relative to each other.

Other considerations

There are several striking differences in this model from the existing models of *h*NHE1 (Landau et al. 2007; Nygaard et al. 2011). First is the position of TM1 in the dimerization domain. This position is based on protein–protein docking although it is noteworthy that in bacterial Na^+/H^+ antiporter structures, the first TM segment is also an integral part of the dimerization domain (C. Lee et al. 2013; Paulino and Kühlbrandt 2014; Wöhlert et al. 2014). The second difference is the position of reentrant loop EL5 after TM9. As TM9 (Leu336–Met354) is positioned at the dimer interface and TM10 (Ser416–Thr433) is positioned in the transportation domain, it is possible that the 60 amino acids situated between these two helices help span the two domains. As noted above, a large preponderance of biochemical data has placed this segment on the extracellular surface (Wakabayashi et al. 2000; Liu et al. 2015). To demonstrate this in the model, Fig. 2F illustrates the amino acids in the model that have been shown earlier in previous publications (Wakabayashi et al. 2000; Slepkov et al. 2005; Reddy et al. 2008; Tzeng et al. 2010; Liu et al. 2015) to be surface accessible and active when mutated to Cys. These experiments were done in earlier publications by biotinylating cell surface proteins and examining the percentage of immunoprecipitated NHE1 protein on the cell surface. Surface accessible residues of NHE1 were almost invariably positioned on the extracellular face of our model on what is predicted to be ELs of the protein (Fig. 2F). A few, such as Ser351, Phe161, and Ile233, are near the extracellular side of TM helices or possibly are accessible because they are within the extracellular accessible funnel of the protein (Slepkov et al. 2005). Four surface accessible residues, T183, E184, S324, and H325 (Wakabayashi et al. 2000), are positioned on intracellular loops. This occurs even though nearby residues are not surface accessible. It was earlier (Wakabayashi et al. 2000) suggested that these residues are part of the structure of the NHE1 pore making them accessible from the extracellular surface. For amino acids 183 and 184, this seems to be supported by the model structure, as they are immediately following TM4 and could be in alignment with the pathway of cations. Amino acids 324 and 325 are not as apparently involved in the cation transport pathway but reside on a long unstructured intracellular loop and could adopt a conformation near the intracellular side of the transport pathway. Some mutations of this intracellular loop compromise activity of the protein (Liu et al. 2015).

Another difference between this model and other ones is in the TM segments making up the Na^+/H^+ exchanger fold. Others have reported that TM4 and TM11 make up the NhaA transportation fold (Hunte et al. 2005; C. Lee et al. 2013; Paulino and Kühlbrandt 2014; Wöhlert et al. 2014). Here, we show that while there is such a fold (Fig. 2E), interestingly, it is made up of TM6 (227–248) and TM11 (Lys447–Leu468). TM4 (155–182) is also a discontinuous helix but does not interact with TM11 to make a typical fold. TM4, while still being a discontinuous helix, is near the NhaA fold but the N-terminal half of the helix extends upward and possibly out of the membrane domain. The suggestion that TM6 is part of the critical fold is supported by results of sequence alignment (Dutta and Fliegel 2018). Additionally, we earlier showed that TM6 is a discontinuous pore lining helix (Tzeng et al. 2011).

Docking of Na^+/H^+ exchanger inhibitors

Docking results identified two putative EIPA interacting sites with relatively close affinities. These sites are named "site A" and "site B". Site A (Fig. 4; Supplementary Fig. 2S[2] and Table 1S[2]) was the most favorable position (for EIPA) with an affinity of −6.4 kcal/mol. It was located in close proximity to the residues of EL5 (Tyr381, Leu383, and Trp386) and TM9 (Phe348 and Ser351) and situated approximately 4.8 Å distance from the TM4 ^{60}VFFLFLLPPIIL^{171} region. At site B (Fig. 2S[2] and Table 1S[2]) (affinity −6.1 kcal/mol), EIPA is more closely associated with the TM4 region. Residues like Phe155 and Asp159 interact directly with EIPA and these residues are located in TM4. EIPA at this site also interacts with the C-terminal side of the EL5. Here, Phe413 (EL5) may be interacting with the pyrazine aromatic ring of EIPA (Fig. 4). Gly466-Tyr467-Leu468 stretch that is located at the TM11b. Met476, and Leu481 are located at the region EL6 TM12 region. In all cases, TM4 and EL5 were involved in the interaction between EIPA and NHE1. Similar results were obtained with

Fig. 4. View of EIPA binding sites A and B from the extracellular surface. Amino acids Leu228, Leu229 (TM6), Val272, Leu273, Tyr274, His275 (EL4), Lys379, Ala380, Tyr381 (EL5), Leu465 (TM11), and Pro475 (EL6) are shown in cyan. (A) With entire protein shown. (B and C) Closeups of sites A and B. [Color online.]

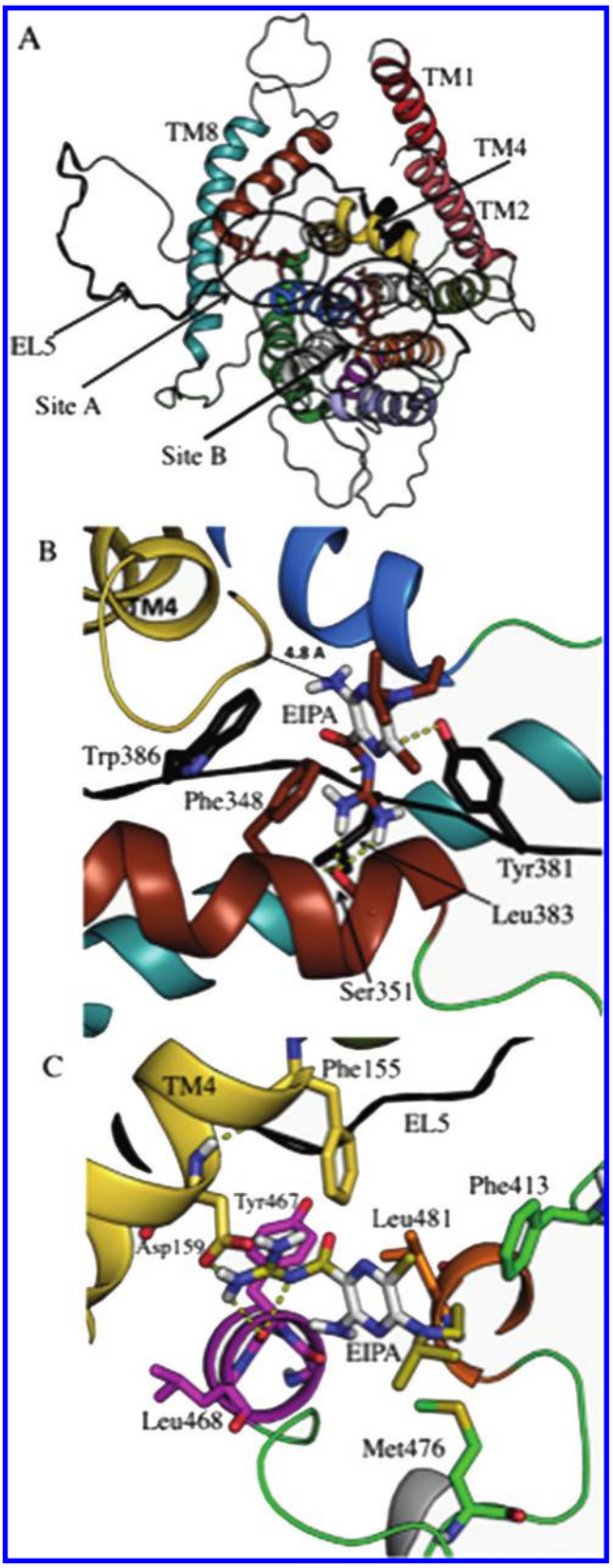

amiloride, cariporide, HMA, and HOE694 (Figs. 3S–10S[2]). Table 1S[2] lists the amino acids in close proximity to various compounds.

Site A is located at the extracellular side of the transport domain and site B is located at the extracellular side of the interface between the scaffolding domain and the transportation domain (Fig. 4). Site A might be the physiological binding site, as it is suggested that amiloride-based inhibitors act through inhibition of the extracellular accessible Na^+ binding site and the trihydrated Na^+ ion is nearly identical in structure to the guanidinium ion of amiloride (Lang 2003).

When mutated, residues of TM4 and His349 of TM9 affect the efficacy of NHE1 inhibitors (Counillon et al. 1993*a*, 1997; Yun et al. 1993; Wang et al. 1995; Lee et al. 2009). We did see some interaction of EIPA with the TM4 segment ^{160}VFFLFLLPPIIL^{171} but not with His349 of TM9. The closest distance from TM4 was with Pro168 that was 4.8 Å from EIPA. However, it has not been shown that EIPA directly binds to this region. In fact, mutations in quite a large number of residues in varied TM segments affect inhibitor potency (Ding et al. 2006; Jinadasa et al. 2015). Some improve and some decrease inhibitor efficacy. It therefore seems likely that these mutations may have subtle effects on the conformation of the protein, thus altering the inhibitor-binding site.

Summary

We present a three-dimensional model of *h*NHE1. The model takes into account empirically determined biochemical data on surface accessibility of the protein in combination with molecular modeling and is based on the structure of *Mj*NhaP1, which is more similar to *h*NHE1 than to NhaA. In this model, TM6 and TM11 form a Na^+/H^+ antiporter fold. Residues 363–410 form EL5, in agreement with Cys accessibility studies that place this segment on the cell surface. A large preponderance of amino acids shown to be accessible on the cell surface are present on the extracellular surface or nearby. Structures of TM segments in the model are similar to the structures of peptides of *h*NHE1 deduced in NMR studies. Preliminary studies examined docking of the Na^+/H^+ exchanger inhibitor EIPA to *h*NHE1 and it is on the extracellular surface in association with several amino acids of different TM regions. Studies are presently underway to determine the three-dimensional structure of inhibitor-bound NHE1 at atomic resolution. Additionally, experiments are underway to examine intramolecular distances with a spin label using the purified cysteineless NHE1 protein with a single or double cysteine introduced.

Acknowledgements

Supported by NSERC grant No. 06564 to L.F.

References

Alves, C., Lee, B.L., Sykes, B.D., and Fliegel, L. 2014. Structural and functional analysis of the transmembrane segment pair VI and VII of the NHE1 isoform of the Na^+/H^+ exchanger. Biochemistry, **53**: 3658–3670. doi:10.1021/bi500392y. PMID:24840010.

Amith, S.R., and Fliegel, L. 2016. The Na^+/H^+ exchanger in metastasis. Aging (Albany NY), **8**: 1291. doi:10.18632/aging.101002.

Amith, S.R., and Fliegel, L. 2017. Na^+/H^+ exchanger-mediated hydrogen ion extrusion as a carcinogenic signal in triple-negative breast cancer etiopathogenesis and prospects for its inhibition in therapeutics. Semin. Cancer Biol. **43**: 35–41. doi:10.1016/j.semcancer.2017.01.004. PMID:28104391.

Amith, S.R., Wilkinson, J.M., and Fliegel, L. 2016. KR-33028, a potent inhibitor of the Na^+/H^+ exchanger NHE1, suppresses metastatic potential of triple-negative breast cancer cells. Biochem. Pharmacol. **118**: 31–39. doi:10.1016/j.bcp.2016.08.010. PMID:27521504.

Brett, C.L., Donowitz, M., and Rao, R. 2005. Evolutionary origins of eukaryotic sodium/proton exchangers. Am. J. Physiol. Cell Physiol. **288**: C223–C239. doi:10.1152/ajpcell.00360.2004. PMID:15643048.

Buchan, D.W., Minneci, F., Nugent, T.C., Bryson, K., and Jones, D.T. 2013. Scalable web services for the PSIPRED Protein Analysis Workbench. Nucleic Acids Res. **41**: W349–W357. doi:10.1093/nar/gkt381. PMID:23748958.

Călinescu, O., Dwivedi, M., Patiño-Ruiz, M., Padan, E., and Fendler, K. 2017. Lysine 300 is essential for stability but not for electrogenic transport of the *Escherichia coli* NhaA Na^+/H^+ antiporter. J. Biol. Chem. **292**: 7932–7941. doi:10.1074/jbc.M117.778175. PMID:28330875.

Counillon, L., Franchi, A., and Pouysségur, J. 1993*a*. A point mutation of the Na^+/H^+ exchanger gene (NHE1) and amplification of the mutated allele confer amiloride resistance upon chronic acidosis. Proc. Natl. Acad. Sci. U.S.A. **90**: 4508–4512. doi:10.1073/pnas.90.10.4508. PMID:8389452.

Counillon, L., Scholz, W., Lang, H.J., and Pouysségur, J. 1993*b*. Pharmacological characterization of stably transfected Na^+/H^+ antiporter isoforms using amiloride analogs and a new inhibitor exhibiting anti-ischemic properties. Mol. Pharmacol. **44**: 1041–1045. PMID:8246907.

Counillon, L., Pouysségur, J., and Reithmeier, R.A. 1994. The Na^+/H^+ exchanger NHE-1 possesses N- and O-linked glycosylation restricted to the first N-terminal extracellular domain. Biochemistry, **33**: 10463–10469. doi:10.1021/bi00200a030. PMID:8068684.

Counillon, L., Noël, J., Reithmeier, R.A., and Pouysségur, J. 1997. Random mutagenesis reveals a novel site involved in inhibitor interaction within the fourth transmembrane segment of the Na^+/H^+ exchanger-1. Biochemistry, **36**: 2951–2959. doi:10.1021/bi9615405. PMID:9062125.

Ding, J., Rainey, J.K., Xu, C., Sykes, B.D., and Fliegel, L. 2006. Structural and functional characterization of transmembrane segment VII of the Na^+/H^+ exchanger isoform 1. J. Biol. Chem. **281**: 29817–29829. doi:10.1074/jbc.M606152200. PMID:16861220.

Dutta, D., and Fliegel, L. 2018. Structure and function of yeast and fungal Na^+/H^+ antiporters. IUBMB Life, **70**: 23–31. doi:10.1002/iub.1701. PMID:29219228.

Dutta, D., Shin, K., Rainey, J.K., and Fliegel, L. 2017. Transmembrane segment XI of the Na^+/H^+ antiporter of *S. pombe* is a critical part of the ion translocation pore. Sci. Rep. **7**: 12793. doi:10.1038/s41598-017-12701-z. PMID:29038548.

Emsley, P., Lohkamp, B., Scott, W.G., and Cowtan, K. 2010. Features and development of Coot. Acta Crystallogr. D Biol. Crystallogr. **66**: 486–501. doi:10.1107/S0907444910007493. PMID:20383002.

Fafournoux, P., Noël, J., and Pouysségur, J. 1994. Evidence that Na^+/H^+ exchanger isoforms NHE1 and NHE3 exist as stable dimers in membranes with a high degree of specificity for homodimers. J. Biol. Chem. **269**: 2589–2596. PMID:8300588.

Fliegel, L. 1999. Functional and cellular regulation of the myocardial Na^+/H^+ exchanger. J. Thromb. Thrombolysis, **8**: 9–14. doi:10.1023/A:1008934312429. PMID:10481209.

Fliegel, L. 2005. The Na^+/H^+ exchanger isoform 1. Int. J. Biochem. Cell Biol. **37**: 33–37. doi:10.1016/j.biocel.2004.02.006. PMID:15381146.

Fliegel, L., Sardet, C., Pouysségur, J., and Barr, A. 1991. Identification of the protein and cDNA of the cardiac Na^+/H^+ exchanger. FEBS Lett. **279**: 25–29. doi:10.1016/0014-5793(91)80241-T. PMID:1704856.

Fliegel, L., Dyck, J.R.B., Wang, H., Fong, C., and Haworth, R.S. 1993. Cloning and analysis of the human myocardial Na^+/H^+ exchanger. Mol. Cell. Biochem. **125**: 137–143. doi:10.1007/BF00936442. PMID:8283968.

França, T.C. 2015. Homology modeling: an important tool for the drug discovery. J. Biomol. Struct. Dyn. **33**: 1780–1793. doi:10.1080/07391102.2014.971429. PMID:25266493.

Goswami, P., Paulino, C., Hizlan, D., Vonck, J., Yildiz, Ö., and Kühlbrandt, W. 2011. Structure of the archaeal Na^+/H^+ antiporter NhaP1 and functional role of transmembrane helix 1. EMBO J. **30**: 439–449. doi:10.1038/emboj.2010.321. PMID:21151096.

Haworth, R.S., Fröhlich, O., and Fliegel, L. 1993. Multiple carbohydrate moieties on the Na^+/H^+ exchanger. Biochem. J. **289**: 637–640. doi:10.1042/bj2890637. PMID:8382044.

Hellmer, J., Pätzold, R., and Zeilinger, C. 2002. Identification of a pH regulated Na^+/H^+ antiporter of *Methanococcus jannaschii*. FEBS Lett. **527**: 245–249. doi:10.1016/S0014-5793(02)03244-1. PMID:12220668.

Hendus-Altenburger, R., Kragelund, B.B., and Pedersen, S.F. 2014. Structural dynamics and regulation of the mammalian SLC9A family of Na^+/H^+ exchangers. Curr. Top. Membr. **73**: 69–148. doi:10.1016/B978-0-12-800223-0.00002-5. PMID:24745981.

Hisamitsu, T., Ben Ammar, Y., Nakamura, T.Y., and Wakabayashi, S. 2006. Dimerization is crucial for the function of the Na^+/H^+ exchanger NHE1. Biochemistry, **45**: 13346–13355. doi:10.1021/bi0608616. PMID:17073455.

Hofmann, K., and Stoffel, W. 1993. TMBASE — a database of membrane spanning protein segments. Biol. Chem. Hoppe-Seyler, **374**: 166.

Huang, Y., Chen, W., Dotson, D.L., Beckstein, O., and Shen, J. 2016. Mechanism of pH-dependent activation of the sodium-proton antiporter NhaA. Nat. Commun. **7**: 12940. doi:10.1038/ncomms12940. PMID:27708266.

Hunte, C., Screpanti, E., Venturi, M., Rimon, A., Padan, E., and Michel, H. 2005. Structure of a Na^+/H^+ antiporter and insights into mechanism of action and regulation by pH. Nature, **435**: 1197–1202. doi:10.1038/nature03692. PMID:15988517.

Jinadasa, T., Josephson, C.B., Boucher, A., and Orlowski, J. 2015. Determinants of cation permeation and drug sensitivity in predicted transmembrane helix 9 and adjoining exofacial re-entrant loop 5 of Na^+/H^+ exchanger NHE1. J. Biol. Chem. **290**: 18173–18186. doi:10.1074/jbc.M115.642199. PMID:26063808.

Kaczor, A.A., Selent, J., Sanz, F., and Pastor, M. 2013. Modeling complexes of transmembrane proteins: systematic analysis of protein–protein docking tools. Mol. Inform. **32**: 717–733. doi:10.1002/minf.201200150. PMID:27480064.

Karmazyn, M. 2013. NHE-1: still a viable therapeutic target. J. Mol. Cell. Cardiol. **61**: 77–82. doi:10.1016/j.yjmcc.2013.02.006. PMID:23429008.

Karmazyn, M., Gan, T.X., Humphreys, R.A., Yoshida, H., and Kusumoto, K. 1999. The myocardial Na^+-H^+ exchange. Structure, regulation, and its role in heart disease. Circ. Res. **85**: 777–786. PMID:10532945.

Katoh, K., and Standley, D.M. 2013. MAFFT multiple sequence alignment software version 7: improvements in performance and usability. Mol. Biol. Evol. **30**: 772–780. doi:10.1093/molbev/mst010. PMID:23329690.

Khadilkar, A., Iannuzzi, P., and Orlowski, J. 2001. Identification of sites in the second exomembrane loop and ninth transmembrane helix of the mammalian Na^+/H^+ exchanger important for drug recognition and cation translocation. J. Biol. Chem. **276**: 43792–43800. doi:10.1074/jbc.M106659200. PMID:11564737.

Kühlbrandt, W., Zeelen, J., and Dietrich, J. 2002. Structure, mechanism, and regulation of the *Neurospora* plasma membrane H+ATPase. Science, **297**: 1692–1696. doi:10.1126/science.1072574. PMID:12169656.

Landau, M., Herz, K., Padan, E., and Ben-Tal, N. 2007. Model structure of the Na^+/H^+ exchanger 1 (NHE1): functional and clinical implications. J. Biol. Chem. **282**: 37854–37863. doi:10.1074/jbc.M705460200. PMID:17981808.

Lang, H.J. 2003. Chemistry of NHE inhibitors. *In* The sodium–hydrogen exchanger: from molecular to its role in disease. *Edited by* M. Karmazyn, M. Avkiran, and L. Fliegel. Springer, Boston. pp. 239–253. doi:10.1007/978-1-4615-0427-6_16.

Lee, B.L., Li, X., Liu, Y., Sykes, B.D., and Fliegel, L. 2009. Structural and functional analysis of transmembrane XI of the NHE1 isoform of the Na^+/H^+ exchanger. J. Biol. Chem. **284**: 11546–11556. doi:10.1074/jbc.M809201200. PMID:19176522.

Lee, B.L., Sykes, B.D., and Fliegel, L. 2013. Structural and functional insights into the cardiac Na^+/H^+ exchanger. J. Mol. Cell. Cardiol. **61**: 60–67. doi:10.1016/j.yjmcc.2012.11.019. PMID:23220151.

Lee, C., Kang, H.J., von Ballmoos, C., Newstead, S., Uzdavinys, P., Dotson, D.L., et al. 2013. A two-domain elevator mechanism for sodium/proton antiport. Nature, **501**: 573–577. doi:10.1038/nature12484. PMID:23995679.

Lee, S.H., Kim, T., Park, E.S., Yang, S., Jeong, D., Choi, Y., and Rho, J. 2008. NHE10, a novel osteoclast-specific member of the Na^+/H^+ exchanger family, regulates osteoclast differentiation and survival [corrected]. Biochem. Biophys. Res. Commun. **369**: 320–326. doi:10.1016/j.bbrc.2008.01.168. PMID:18269914.

Liu, Y., Basu, A., Li, X., and Fliegel, L. 2015. Topological analysis of the Na^+/H^+ exchanger. Biochim. Biophys. Acta Biomembr. **1848**: 2385–2393. doi:10.1016/j.bbamem.2015.07.011. PMID:26215741.

Lovell, S.C., Davis, I.W., Arendall, W.B., 3rd, de Bakker, P.I., Word, J.M., Prisant, M.G., et al. 2003. Structure validation by Calpha geometry: phi,psi and Cbeta deviation. Proteins, **50**: 437–450. doi:10.1002/prot.10286. PMID:12557186.

Möller, S., Croning, M.D., and Apweiler, R. 2001. Evaluation of methods for the prediction of membrane spanning regions. Bioinformatics, **17**: 646–653. doi:10.1093/bioinformatics/17.7.646. PMID:11448883.

Moncoq, K., Kemp, G., Li, X., Fliegel, L., and Young, H.S. 2008. Dimeric structure of human Na^+/H^+ exchanger isoform 1 overproduced in *Saccharomyces cerevisiae*. J. Biol. Chem. **283**: 4145–4154. doi:10.1074/jbc.M704844200. PMID:18077454.

Morris, G.M., Huey, R., Lindstrom, W., Sanner, M.F., Belew, R.K., Goodsell, D.S., and Olson, A.J. 2009. AutoDock4 and AutoDockTools4: automated docking with selective receptor flexibility. J. Comput. Chem. **30**: 2785–2791. doi:10.1002/jcc.21256. PMID:19399780.

Nygaard, E.B., Lagerstedt, J.O., Bjerre, G., Shi, B., Budamagunta, M., Poulsen, K.A., et al. 2011. Structural modeling and electron paramagnetic resonance spectroscopy of the human Na^+/H^+ exchanger isoform 1, NHE1. J. Biol. Chem. **286**: 634–648. doi:10.1074/jbc.M110.159202. PMID:20974853.

Olkhova, E., Hunte, C., Screpanti, E., Padan, E., and Michel, H. 2006. Multiconformation continuum electrostatics analysis of the NhaA Na^+/H^+ antiporter of *Escherichia coli* with functional implications. Proc. Natl. Acad. Sci. U.S.A. **103**: 2629–2634. doi:10.1073/pnas.0510914103. PMID:16477015.

Orlowski, J., and Grinstein, S. 2004. Diversity of the mammalian sodium/proton exchanger SLC9 gene family. Pflugers Arch. **447**: 549–565. doi:10.1007/s00424-003-1110-3. PMID:12845533.

Orlowski, J., Kandasamy, R.A., and Shull, G.E. 1992. Molecular cloning of putative members of the Na^+/H^+ exchanger gene family. J. Biol. Chem. **267**: 9331–9339. PMID:1577762.

Padan, E. 2014. Functional and structural dynamics of NhaA, a prototype for Na^+ and H^+ antiporters, which are responsible for Na^+ and H^+ homeostasis in cells. Biochim. Biophys. Acta Bioenerg. **1837**: 1047–1062. doi:10.1016/j.bbabio.2013.12.007. PMID:24361841.

Padan, E., Danieli, T., Keren, Y., Alkoby, D., Masrati, G., Haliloglu, T., et al. 2015. NhaA antiporter functions using 10 helices, and an additional 2 contribute to assembly/stability. Proc. Natl. Acad. Sci. U.S.A. **112**: E5575–E5582. doi:10.1073/pnas.1510964112. PMID:26417087.

Paulino, C., and Kühlbrandt, W. 2014. pH- and sodium-induced changes in a sodium/proton antiporter. eLife, **3**: e01412. doi:10.7554/eLife.01412. PMID:24473071.

Pedersen, S.F., King, S.A., Nygaard, E.B., Rigor, R.R., and Cala, P.M. 2007. NHE1 inhibition by amiloride- and benzoylguanidine-type compounds. Inhibitor binding loci deduced from chimeras of NHE1 homologues with endogenous differences in inhibitor sensitivity. J. Biol. Chem. **282**: 19716–19727. PMID:17493937.

Pettersen, E.F., Goddard, T.D., Huang, C.C., Couch, G.S., Greenblatt, D.M., Meng, E.C., and Ferrin, T.E. 2004. UCSF Chimera — a visualization system for

exploratory research and analysis. J. Comput. Chem. **25**: 1605–1612. doi:10.1002/jcc.20084. PMID:15264254.

Rashid, M.H., and Kuyucak, S. 2012. Affinity and selectivity of ShK toxin for the Kv1 potassium channels from free energy simulations. J. Phys. Chem. B, **116**: 4812–4822. doi:10.1021/jp300639x. PMID:22480371.

Reddy, T., Ding, J., Li, X., Sykes, B.D., Rainey, J.K., and Fliegel, L. 2008. Structural and functional characterization of transmembrane segment IX of the NHE1 isoform of the Na^+/H^+ exchanger. J. Biol. Chem. **283**: 22018–22030. doi:10.1074/jbc.M803447200. PMID:18508767.

Reshkin, S.J., Greco, M.R., and Cardone, R.A. 2014. Role of pHi, and proton transporters in oncogene-driven neoplastic transformation. Philos. Trans. R. Soc. Lond. B Biol. Sci. **369**: 20130100. doi:10.1098/rstb.2013.0100. PMID:24493748.

Rimon, A., Tzubery, T., and Padan, E. 2007. Monomers of the NhaA Na^+/H^+ antiporter of *Escherichia coli* are fully functional yet dimers are beneficial under extreme stress conditions at alkaline pH in the presence of Na^+ or Li^+. J. Biol. Chem. **282**: 26810–26821. doi:10.1074/jbc.M704469200. PMID:17635927.

Rimon, A., Kozachkov-Magrisso, L., and Padan, E. 2012. The unwound portion dividing helix IV of NhaA undergoes a conformational change at physiological pH and lines the cation passage. Biochemistry, **51**: 9560–9569. doi:10.1021/bi301030x. PMID:23131124.

Šali, A., and Blundell, T.L. 1993. Comparative protein modelling by satisfaction of spatial restraints. J. Mol. Biol. **234**: 779–815. doi:10.1006/jmbi.1993.1626. PMID:8254673.

Slepkov, E.R., Rainey, J.K., Li, X., Liu, Y., Cheng, F.J., Lindhout, D.A., et al. 2005. Structural and functional characterization of transmembrane segment IV of the NHE1 isoform of the Na^+/H^+ exchanger. J. Biol. Chem. **280**: 17863–17872. doi:10.1074/jbc.M409608200. PMID:15677483.

Slepkov, E., Ding, J., Han, J., and Fliegel, L. 2007. Mutational analysis of potential pore-lining amino acids in TM IV of the Na^+/H^+ exchanger. Biochim. Biophys. Acta Biomembr. **1768**: 2882–2889. doi:10.1016/j.bbamem.2007.08.011. PMID:17935692.

Takaichi, K., Wang, D., Balkovetz, D.F., and Warnock, D.G. 1992. Cloning, sequencing, and expression of Na^+/H^+ antiporter cDNAs from human tissues. Am. J. Physiol. Cell Physiol. **262**: C1069–C1076. doi:10.1152/ajpcell.1992.262.4.C1069. PMID:1314485.

Touret, N., Poujeol, P., and Counillon, L. 2001. Second-site revertants of a low-sodium-affinity mutant of the Na^+/H^+ exchanger reveal the participation of TM4 into a highly constrained sodium-binding site. Biochemistry, **40**: 5095–5101. doi:10.1021/bi0025464. PMID:11305927.

Trott, O., and Olson, A.J. 2010. AutoDock Vina: improving the speed and accuracy of docking with a new scoring function, efficient optimization, and multithreading. J. Comput. Chem. **31**: 455–461. doi:10.1002/jcc.21334. PMID:19499576.

Tzeng, J., Lee, B.L., Sykes, B.D., and Fliegel, L. 2010. Structural and functional analysis of transmembrane segment VI of the NHE1 isoform of the Na^+/H^+ exchanger. J. Biol. Chem. **285**: 36656–36665. doi:10.1074/jbc.M110.161471. PMID:20843797.

Tzeng, J., Lee, B.L., Sykes, B.D., and Fliegel, L. 2011. Structural and functional analysis of critical amino acids in TMVI of the NHE1 isoform of the Na^+/H^+ exchanger. Biochim. Biophys. Acta Biomembr. **1808**: 2327–2335. doi:10.1016/j.bbamem.2011.05.004. PMID:21600870.

Ullah, A., Kemp, G., Lee, B., Alves, C., Young, H., Sykes, B.D., and Fliegel, L. 2013. Structural and functional analysis of transmembrane segment IV of the salt tolerance protein Sod2. J. Biol. Chem. **288**: 24609–24624. doi:10.1074/jbc.M113.483065. PMID:23836910.

Ullah, A., Dutta, D., and Fliegel, L. 2016. Expression and characterization of the SOS1 *Arabidopsis* salt tolerance protein. Mol. Cell. Biochem. **415**: 133–143. doi:10.1007/s11010-016-2685-2. PMID:26992907.

van Zundert, G.C.P., Rodrigues, J.P.G.L.M., Trellet, M., Schmitz, C., Kastritis, P.L., Karaca, E., et al. 2016. The HADDOCK2.2 web server: user-friendly integrative modeling of biomolecular complexes. J. Mol. Biol. **428**: 720–725. doi:10.1016/j.jmb.2015.09.014. PMID:26410586.

Wakabayashi, S., Pang, T., Su, X., and Shigekawa, M. 2000. A novel topology model of the human Na^+/H^+ exchanger isoform 1. J. Biol. Chem. **275**: 7942–7949. doi:10.1074/jbc.275.11.7942. PMID:10713111.

Wang, D., Balkovetz, D.F., and Warnock, D.G. 1995. Mutational analysis of transmembrane histidines in the amiloride-sensitive Na^+/H^+ exchanger. Am. J. Physiol. Cell Physiol. **269**: C392–C402. doi:10.1152/ajpcell.1995.269.2.C392. PMID:7653521.

Wöhlert, D., Kühlbrandt, W., and Yildiz, Ö . 2014. Structure and substrate ion binding in the sodium/proton antiporter PaNhaP. eLife, **3**: e03579. doi:10.7554/eLife.03579. PMID:25426802.

Xu, D., and Zhang, Y. 2011. Improving the physical realism and structural accuracy of protein models by a two-step atomic-level energy minimization. Biophys. J. **101**: 2525–2534. doi:10.1016/j.bpj.2011.10.024. PMID:22098752.

Yun, C.H., Little, P.J., Nath, S.K., Levine, S.A., Pouysségur, J., Tse, C.M., and Donowitz, M. 1993. Leu143 in the putative fourth membrane spanning domain is critical for amiloride inhibition of an epithelial Na^+/H^+ exchanger isoform (NHE-2). Biochem. Biophys. Res. Commun. **193**: 532–539. doi:10.1006/bbrc.1993.1656. PMID:8512555.

This article has been cited by:

1. Larry Fliegel. 2019. Structural and Functional Changes in the Na+/H+ Exchanger Isoform 1, Induced by Erk1/2 Phosphorylation. *International Journal of Molecular Sciences* **20**:10, 2378. [Crossref]

Inhibitor	Sites	Residues involved	Affinity kcal/mol	Remarks
Amiloride	Site A	Asp172, Phe348, Ser351, Tyr381, Phe382, Lys384, Trp386	-5.6	TM4, TM9, EL5
	Site B	Phe155, Asp159, Tyr467, Asp470, Met476	-5.6	TM4, TM11, EL6
Cariporide	Site A	Val271, Phe348, Ser351, Trp386, Tyr381, Leu383	-7.6	EL5, TM7-EL4, TM9
	Site B	Phe155, Asp159, Phe413, His407, His408, Asp470	-7.7	TM4, C-terminal of EL5, TM11, EL6,
EIPA	Site A	Phe348, Ser351, Tyr381, Leu383, Trp386	-6.4	TM9, EL5, within 4.8Å distance with TM4 ^{60}VFFLFLLPPIIL^{171} region
	Site B	Phe155, Asp159, Phe413, Gly466, Tyr467, Leu468, Met476, Leu481,	-5.9	TM4, C-terminal of EL5, TM11b, EL6, N-terminal of TM12
HMA	Site A	Asp172, Pro167, Ser232, Val272, Phe348, Tyr381, Leu465,	-6.8	TM4, TM6, TM7-EL4, TM9, EL5, TM11
	Site B	Phe155, Asp159, Phe413, Tyr467, His473, Met476, Leu481	-6.8	TM4, C-terminal of EL5, EL6,
HOE694	Site A	Pro167, Phe348, Ser351, Gly352, Leu468, Leu465	-7.6	TM4, TM9, TM11
	Site B	Phe155, His408, Phe413, Asp470, Met476	-7.2	TM4, EL5, EL6

Table 1S: Residues involved in sites of NHE1 inhibitor binding within 3.5 Å except where indicated. "-" indicates connection between TM7 and EL4 where indicated.